Effect of a *p*-6P Induced Layer on the Optoelectronic Performance of Organic Field-Effect Transistors

Wenwen Li [1, a], Shiguang Li [1, b, *], Zhao Zhang [1, c], Zitong Wang [1, d]

[1] College of Automation and Information Engineering, Xi'an University of Technology, Xi'an, China;

[a] liwenwenxaut@163.com, [b] lisg@xaut.edu.cn, [c] 313724950@qq.com, [d] 2250130609@qq.com

Abstract. This study investigated the electrical and photosensitive properties of organic field-effect transistors (OFETs) using para-hexaphenyl (*p*-6P) as induction layers. The widely researched pentacene was employed as the active layer in these devices. Pentacene thin films were epitaxially grown on *p*-6P template layers, which effectively reduced interfacial disorder and increased the crystalline domain size. Consequently, the pentacene/*p*-6P transistors exhibited high-quality saturation characteristics along with a negative shift threshold voltage, resulting in a significant enhancement in on-current and a reduction in turn-on voltage. Furthermore, the thickness dependence of template layers on device performance was systematically investigated. At *p*-6P thickness of 4 nm, Hole mobility increased to 0.1452 $cm^2 V^{-1} s^{-1}$, which was about 7 times higher than that of the device without inducted layer (0 nm), The threshold voltage was reduced from -24 V to -6 V. A maximum photoresponsivity (Rm_{ax}) of 1.72 A/W was achieved. Therefore, these results demonstrate that the *p*-6P template layer provides an effective approach for significantly enhancing the performance of OFETs, offering valuable insights for future device optimization through interfacial engineering.

Keywords: OFET; template layers; Photosensitivity.

1. Introduction

OFETs has the advantages of low processing cost, good mechanical flexibility, biocompatibility and good ductility. They are widely used in many fields, such as wearable devices[1] sensing devices [2], solar cells[3], sustainable electronics[4,5], biosensing[6,7]. Organic photodetectors based on OFETs (referred to as organic phototransistors) generally exhibit higher sensitivity and lower noise compared to photodiodes[8]. As a typical type organic semiconductor material, pentacene has attracted much attention due to its high carrier mobility and good environmental stability[9]. However, pentacene films usually exhibit a polycrystalline structure with small grain sizes and random orientation, leading to high grain boundary density and significantly limiting carrier transport efficiency and device performance[10]. Research shows that the charge transport properties of organic semiconductors are highly dependent on the crystallinity of the films and the quality of the interfaces, especially the initial molecular arrangement near the insulating layer[11,12]. Therefore, optimizing the ordered growth of the semiconductor layer through interface engineering has become one of the key strategies to enhance OFET performance.

In recent years, the weak epitaxy growth (WEG) technique induced by molecular templates has been proven to effectively regulate the film morphology of organic semiconductors. For example, *p*-6P, as a rigid aromatic molecule, has a regularly arranged lattice that can serve as a template for inducing highly ordered growth of semiconductor materials such as copper phthalocyanine[13]. Qian et al.[13] utilized a *p*-6P template layer to fabricate CuPc/*p*-6P heterojunction phototransistors, discovering that *p*-6P not only reduced the grain boundary defects of CuPc through geometric channel effects but also significantly enhanced the efficiency of photo-induced charge carrier separation. Similarly, Tang et al.[14] applied *p*-6P in pentacene OFETs and found that the *p*-6P-induced layer notably improved the crystallinity of pentacene.

Based on this, this study proposes introducing *p*-6P as an inducing layer into pentacene OFETs, regulating the film morphology of pentacene through WEG technique, and investigating its impact on the optoelectronic properties of the devices. When the thickness of the *p*-6P inducing layer was 4 nm, The hole mobility of the device increases from 0.0241 $cm^2 V^{-1} s^{-1}$ to 0.1452 $cm^2 V^{-1} s^{-1}$,

Threshold voltage dropped from -24 V to -8 V, and the photosensitivity was enhanced to 1.72 A/W. These results provide theoretical support for studying the influence of inducing layers on the optoelectronic properties of OFETs.

2. Experimental

2.1 Materials

Pentacene (purity>99.7%) and *p*-6P (purity 95%) were purchased from Sinopharm Chemical Reagent Co., Ltd. The molecular structure is shown in Fig. 1. All materials were used as received without further purification.

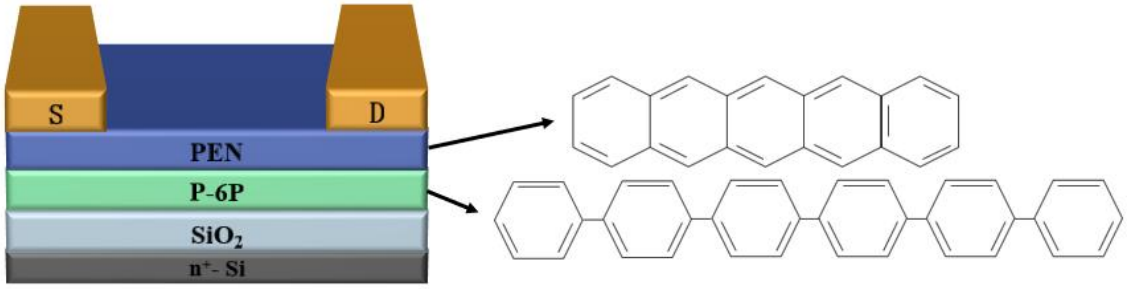

Fig. 1 Molecular structure diagram and OFET structure diagram of pentacene and *p*-6P

2.2 Device fabrication

Fig. 1 shows the device structure of the OFET, It is a bottom-gate-top contact structure. The device is processed as follows: The N-type silicon substrate is ultrasonically cleaned with acetone, ethanol, and water for 10 minutes in sequence. Subsequently, different thicknesses (0, 2, 4, 6 nm) of *p*-6P are deposited using a vacuum evaporation system to form the induction layer. After that, pentacene is deposited on the device using the vacuumevaporation system again to form the active layer. Finally, 80 nm thick Cu is thermally evaporated onto the active layer to serve as the source and drain electrodes

2.3 Film characterization

The film composition and crystal structure information were analyzed using an X-ray crystal instrument (XRD). The electrical and optical characteristics of devices with induced layers of different thicknesses (0, 2, 4, 6 nm) were tested using a Keithley 2636 semiconductor tester. The morphology of the film was characterized using an atomic force microscope (AFM), and the UV Vis absorption spectra of the films were measured.

3. Results and discussions

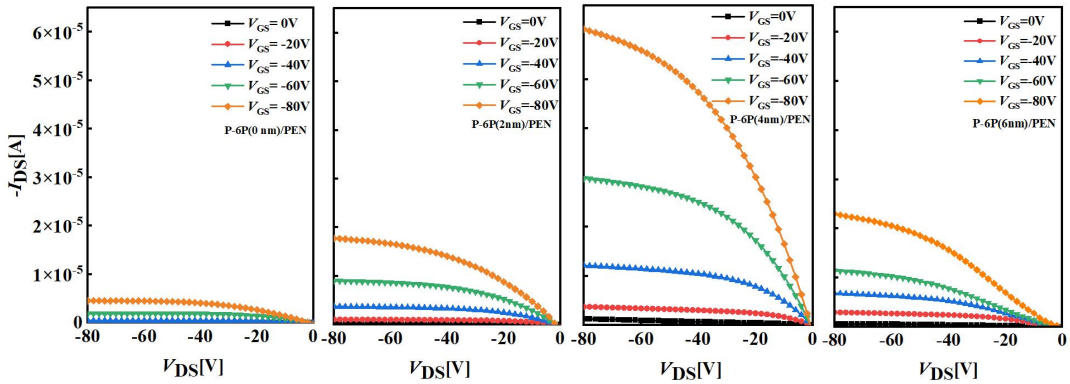

Fig. 2 Output characteristic of devices with different induced layers(0 nm,2 nm,4 nm,6 nm)

Firstly, the influence of depositing different thicknesses of *p*-6P induction layers on the electrical parameters of the devices was studied. Fig. 2 shows the output characteristic curves of devices with different thicknesses of induction layers. It can be seen from Fig.2 that all devices exhibit P-type FET characteristics. Moreover, the deposition of the induction layer remarkably increases the saturation current. The degree of change varies with different film thicknesses. The device with a 4 nm induction layer has the largest saturation current, reaching 12 times that of the device without induced layer, approaching 60 μA. The average values of the electrical parameters of twenty devices are summarized in Table 1.

Tab 1. Electrical performance of devices with different thickness induced layers

Thickness (nm)	μ_{Dark} ($cm^2\ V^{-1}\ s^{-1}$)	$I_{DS(sat)}$ (μA)	V_{TH} (V)
0	0.0241	4.76	-24
2	0.0433	18.21	-10
4	0.1452	58.08	-6
6	0.0513	23.75	-8

It can be seen from Table 1 that the electrical performance of OFETs after all the deposition of the induction layer films is higher than that of the devices without the induction layer. Among them, the device with a thickness of 4 nm is particularly prominent, with a carrier mobility of 0.1452 $cm^2\ V^{-1}\ s^{-1}$, which is 7 times that of the original device. At the same time, the threshold voltage also significantly decreases, from -24 V to -6 V, indicating that the device can operate at a lower voltage and has lower power consumption. Similarly, the electrical performance of the 6 nm device also improves, with a mobility of 0.0513 $cm^2\ V^{-1}\ s^{-1}$ and a decreased threshold voltage. The reason for this phenomenon may be related to the order and roughness of the film.

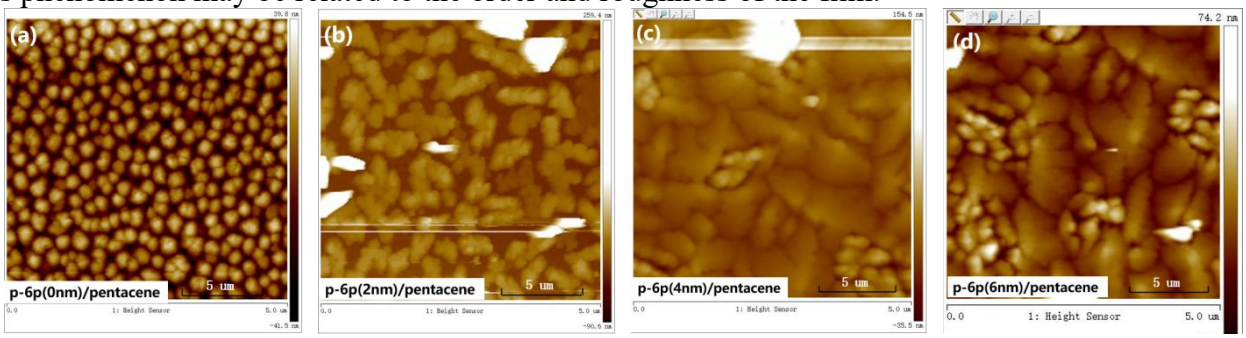

Fig. 3 Morphology of 30nm pentacene films deposited on *p*-6P of different thicknesses (a)0 nm, (b)2 nm, (c)4 nm, (d)6 nm

In order to study the influence of thin films on the performance of different devices, pentacene thin films deposited on *p*-6P of different thicknesses were prepared. The undeposited induction layer is shown in Fig. 3 (a). pentacene is directly generated on the surface of SiO_2, and forms an approximately hexagonal island structure. The resulting grain size is relatively small, approximately 150nm. The small grain size also leads to a larger grain boundary area and a relatively large spacing between grains. The Roughness Average (Ra) of the pentacene film reached 9.39 nm. When the thickness of the induction layer was 2 nm, the grain size of pentacene increased significantly, as shown in Fig. 3 (b), with the average size reaching 500nm. The surface roughness Ra of the film decreased to 6.7 nm, indicating that *p*-6P played an inducing role in the growth of the pentacene film. However, the grain arrangement in the film was not tight enough, and the grain boundary gap had a relatively large size. Severe scattering occurs when carriers pass through grain boundaries. The morphology of pentacene deposited on the 4 nm thick induction layer is the best, and the roughness of the film surface is 4.84 nm, as shown in Fig. 3 (c). The induction effect of the *p*-6P film is the most significant. The grain size is remarkably increased to the micrometer level. The internal lattice structure of pentacene grains is complete with few defects, which is conducive to the movement of carriers, and the crystal arrangement is extremely tight. The influence of carrier scattering at grain boundaries on transport has been reduced. When depositing the 6nm induction layer, the pentacene film deposited on it is shown in Fig. 3 (d), with a surface roughness Ra of 5.31

nm. However, the grain size of pentacene grown is smaller than that of pentacene grown on the 4 nm induction layer, and a small amount of grain boundary gaps appear. The insufficiently tight arrangement of grains may lead to an increase in defects in the crystal structure. These defects may become traps for carriers, thereby reducing the performance of the device.

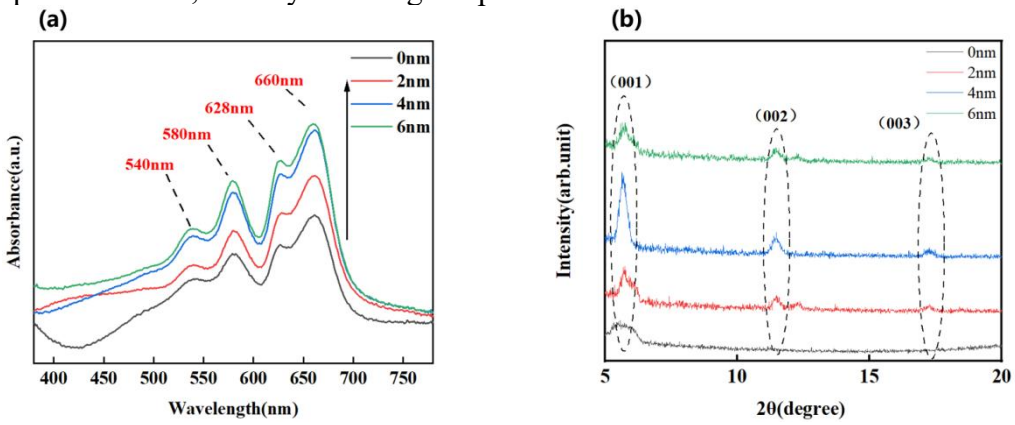

Fig. 4 (a) Absorption spectra of pentacene films deposited on *p*-6P with different thicknesses (b) XRD patterns of pentacene films on different thickness induced layer films

30 nm pentacene films based on different thickness inducing layers were prepared on transparent ITO glass. UV-Vis absorption spectra of different films were characterized. As shown in Fig. 4(a), the pentacene films have very poor spectral stability in the UV region, and the light absorption of pentacene mainly occurs in the visible light region, with absorption peaks at wavelengths of 540 nm, 580 nm, 628 nm, and 660 nm. By adding a *p*-6P inducing layer, the absorption intensity of pentacene/ *p*-6P films notably increases. As the thickness of the *p*-6P inducing layer increases, the absorption intensity of the pentacene/ *p*-6P films gradually increases, with the rate of increase gradually decreasing. XRD analysis was conducted on pentacene films deposited on different thicknesses of *p*-6P, as shown in Fig. 4(b). The intensity of the pentacene film's diffraction peak (001) (2θ = 5.84°) was greater than that of the pentacene film without the induced layer, And with the increase of the thickness of the induction layer, it first increases and then decreases, The maximum value is reached when the thickness of *p*-6P is 4 nm.This indicates that the crystalline order of the pentacene film was remarkably improved, and the 4 nm thick *p*-6P film had a strong templating effect, while the highly ordered pentacene film was beneficial for enhancing the charge transport capability of the device.

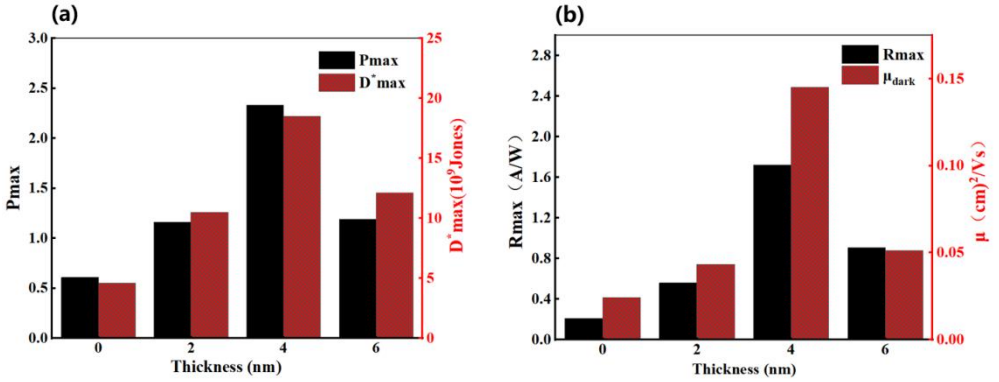

Fig. 5 (a) Relationship between light dark current ratio, specific detection rate and induced layer thickness (b) Relationship between mobility, optical responsivity and induced layer thickness

Fig. 5 shows the variation curves of the device's mobility (μ) under dark conditions, the maximum photo-to-dark current ratio (Pmax) after illumination, the maximum photoresponsivity (R_{MAX}), and the maximum specific detectivity (D^*_{MAX}) with the thickness of the *p*-6P inducing layer (in units of nm). The device's mobility, photo-to-dark current ratio, specific detectivity, and photoresponsivity all increase first and then decrease with the increase in the thickness of the *p*-6P inducing layer. The photosensitive parameters of the devices with inducing layers are all higher than those of the devices with an inducing layer thickness of 0 nm. The 4 nm inducing layer device

has the highest parameters, with a photo-to-dark current ratio reaching 2.33 (under a light intensity of 3.75 mW/cm²) and a photoresponsivity as high as 1.72 A/W.

Tab 2. Photosensitive performance parameters of the different thickness induced layers

Thickness (nm)	light dark current ratio	$R_{MAX)}$ (A/W)	D^*_{MAX} (10^9Jones)
0	0.74	0.21	4.61
2	1.16	0.56	10.5
4	2.33	1.72	18.5
6	1.12	0.98	13.3

The average optical characteristic parameters of 20 devices are summarized, as shown in Table 2. From table 2, it can be found that the photosensitive parameters of the devices are greater than those of the devices with the induced layer thickness of 0nm, the dark current of the devices with the induced layer thickness of 4 nm is higher than that of the original device, and the light dark current ratio is also greater than that of the devices with the induced layer thickness of 0nm, reaching 2.33. The optical loudness of the devices has also been improved, indicating that the deposition of different thickness of the induced layer can improve the ability of the device to convert high light signals into electrical signals, and the 4 nm induced layer device is as high as 1.72 A/W. The improvement of the electrical characteristics of the device is attributed to the fact that the pentacene film can be epitaxially grown on the surface of *p*-6P film to form a highly ordered film. The highly ordered pentacene film with large grain size can greatly improve the charge transport, thus improving the performance of the device[13]. The improvement of the optical characteristics of the device is attributed to the increase of the light absorption intensity of *p*-6P/pentacene film due to the addition of the induction layer, resulting in the increase of the total number of photogenerated excitons. The excellent film quality makes the transmission and dissociation of excitons more effective, and the photocurrent is mainly generated in the highly ordered grains, and the photocurrent generated at the boundary between grains can be ignored[13].

4. Summary

This study adopted *p*-6P as the inducing layer and pentacene as the active layer to investigate the optoelectronic properties of OFETs devices under different induction layer thicknesses. The electrical performance of the devices deposited with the induced layer is higher than that of the devices without the induced layer. The device with a thickness of 4 nm is the most prominent. The carrier mobility is 0.1452 $cm^2\ V^{-1}\ s^{-1}$, which is seven times that of the devices without the induced layer. The threshold voltage also decreases significantly, from -24 V to -6 V, indicating that the device has lower working voltage and lower power consumption. The improved electrical performance stems from the *p*-6P layer, which optimizes the grain size and crystallographic order of the pentacene film. This structural refinement facilitates efficient hole transport at the interface, thereby enhancing charge carrier mobility. After depositing the inducing layer, the photoresponsivity of the devices also improved. Depositing inducing layers of different thicknesses enhanced the device's ability to convert light signals into electrical signals. The improvement in optical performance was attributed to an increase in the total number of photo-generated excitons, higher exciton dissociation efficiency, and excitons dissociating under the electric field to form charge carriers for conduction. The 4 nm inducing layer device had the best optical parameters, The light-to-dark current ratio is 2.33 (light intensity of 3.75 mW/cm²) and a high photoresponsivity of 1.72 A/W. Therefore, these results show that *p*-6P as an inductive layer can effectively improve the photoelectric performance of the device.

References

[1] Zhiyuan Tian, Zeyu Zhao, Feng Yan,Organic electrochemical transistor in wearablebioelectronics:Profiles,applications,andintegration,Wearable Electronics,Volume 1,2024,Pages 1-25,ISSN 2950-2357.

[2] Weiqi Wang, Jiamu Cao, Rongji Zhang, Liang Chen, Yang Li, Yufeng Zhang,Design strategies of semiconductor sensors toward ammonia monitoring in smart agriculture,Journal of Environmental Chemical Engineering,Volume 12, Issue 6,2024,114380,ISSN 2213-3437.

[3] Hanan M.F. Elnagdy,4,7-di-(2-thienyl)-2,1,3- benzothiadiazole DTBT as active core for synthesizing small molecules to optoelectronic applications: A review,Dyes and Pigments,Volume 229,2024,112251,ISSN 0143-7208.

[4] G. Konwar, V. Raghuwanshi, P. Saxena, S. Rahi, S. Bhattacharjee and S. P. Tiwari, "Solution Processed Organic Transistors on Paper Substrate for Sustainable Electronics," in IEEE Transactions on Electron Devices, vol. 71, no. 1, pp. 762-768, Jan. 2024.

[5] G. Konwar, S. Rahi and S. P. Tiwari, "Exploration of a Cellulose-Based Biocompatible Gate Dielectric for Low-Voltage Organic Transistors," in IEEE Journal on Flexible Electronics, vol. 2, no. 5, pp. 383-389, Sept. 2023.

[6] A. Ali, A. M. Sallam, M. Mohsen, A. Kasry and S. O. Abdellatif, "Highly Sensitive, Low Operating Power Cardiac Troponin Biosensor Using PANI Nanofiber OFET," in IEEE Transactions on Nanotechnology, vol. 22, pp. 558-563, 2023.

[7] Rosaria Anna Picca, Kyriaki Manoli, Antonio Luciano, Maria Chiara Sportelli, Gerardo Palazzo, Luisa Torsi, Nicola Cioffi, Enhanced stability of organic field-effect transistor biosensors bearing electrosynthesized ZnO nanoparticles,Sensorsand Actuators B: Chemical,Volume 274,2018.

[8] Baeg KJ, Binda M, Natali D, Caironi M, Noh YY. Organic light detectors: photodiodes and phototransistors. Advanced materials. 2013 Aug 21;25(31):4267-95.

[9] Klauk H, Zschieschang U, Pflaum J, Halik M. Ultralow-power organic complementary circuits. nature. 2007 Feb 15;445(7129):745-8.

[10] Stoliar P, Kshirsagar R, Massi M, Annibale P, Albonetti C, De Leeuw DM, Biscarini F. Charge injection across self-assembly monolayers in organic field-effect transistors: Odd− even effects. Journal of the American Chemical Society. 2007 May 23;129(20):6477-84.

[11] Xu Y, Sun H, Liu A, Zhu H, Li B, Minari T, Balestra F, Ghibaudo G, Noh YY. Essential effects on the mobility extraction reliability for organic transistors. Advanced Functional Materials. 2018 Oct;28(42):1803907.

[12] Yang J, Yan D. Weak epitaxy growth of organic semiconductor thin films. Chemical Society Reviews. 2009;38(9):2634-45.

[13] Qian C, Sun J, Kong LA, Gou G, Zhu M, Yuan Y, Huang H, Gao Y, Yang J. High‐performance organic heterojunction phototransistors based on highly ordered copper phthalocyanine/para-sexiphenyl thin films. Advanced Functional Materials. 2017 Feb;27(6):1604933.

[14] Tang Y, Jiang F, Cui X, Wang H. Zero drive load inverter with high gain and large noise margin based on organic weak epitaxy growth method. Journal of Physics D: Applied Physics. 2020 Mar 26;53(22):225101.